

Supporting Information

Electron Spin Density Matching for Cross-Effect Dynamic Nuclear Polarization

Yuanxin Li,[†] Asif Equbal,[†] Kan Tagami,[†] and Songi Han^{*,†,‡}

[†]*Department of Chemistry and Biochemistry, University of California, Santa Barbara,
Santa Barbara, California 93106, United States.*

[‡]*Department of Chemical Engineering, University of California, Santa Barbara, Santa
Barbara, California 93106, United States.*

E-mail: songi@chem.ucsb.edu

Contents

Experimental Methods and Results	2
Static DNP and Pulse EPR	2
Magic-Angle Spinning DNP	3
T _{1e} Relaxation Measurement	3
ELDOR	5
Numerical simulation	6
EPR Spectra	6
CE-DNP Simulation Under MAS	6

Experimental Methods and Results

Static DNP and pulse EPR at 4 K and 6.9 T

4-Amino TEMPO, denoted as TEMPO, (Sigma-Aldrich) and Trityl-OX063, denoted as Trityl, (GE Healthcare AC) with a total radical concentration of 30-53.2 mM were dissolved in DNP-juice, d_8 -glycerol (Cambridge Isotopes): D_2O (Cambridge Isotopes): H_2O (UCSB Lab) = 6:3:1, *vol%*. 40 μ L mixed radical solution was deposited into a cylindrical Teflon sample holder with the following dimensions: 7 mm O.D. and outer height, with 0.5 mm thick walls. The sample holder was inserted into a 294 MHz Alderman-Grant 1H NMR coil which was inductively coupled to a RF pick-up loop. The NMR coil was coupled with NMR probe which has corrugated wave-guide inbuilt. The NMR probe was top-loaded into a customized Janis STVP-NMR wide-bore cryostat and was cooled down to 4 K using a continuous flow of liquid helium. At the bottom of the sample holder, a silver mirror was placed to reflect the μw coming from the corrugated wave-guide to enhance the μw B_1 -field at the sample position. More detailed description of the instrument design can be found in the previous papers from Han Lab.^{1,2} The DNP enhancement ($^1H\epsilon$) obtained with the static-DNP system were recorded using 1H solid-echo detection with a $\pi/2$ pulse-train as the pre-saturation pulse followed by a 60 s μw irradiation. Temperature was measured with a Cernox temperature sensor inside the cryostat at the sample position.

Pulse EPR measurements were conducted with the same setup. μw pulses are generated using the pulse forming unit at ~ 12 GHz, aided with arbitrary wave form generating capability.² Upon pulse formation, the μw pulses were amplified in frequency by a factor of 16, to ~ 200 GHz, with amplitude multiplier chain (AMC). μw irradiation were then guided through Quasi Optics (QO) bridge, which both minimized the loss of μw transmission and allows μw dual-resonance irradiation, for pump-probe EPR experiments. EPR signal was detected at 3 GHz with superheterodyne detection. More details can be found in our previous publications.²⁻⁴

Magic-Angle Spinning DNP at 25 K and 6.9 T

TEMPO and Trityl radicals with a global concentration of 40 mM in DNP-juice was mixed with 0.3 M $2\text{-}^{13}\text{C}$ labeled glycine (Cambridge Isotopes). The mixture was blended with ~ 60 mg dry KBr for the purpose of temperature calibration inside a zirconia rotor obtained from Revolution NMR, which has the following dimension: 4 mm outer-diameter, 2.36 mm inner-diameter, and 46 mm axial-length. The sample position was fixed at the center of the rotor using Teflon-inserts placed at its both ends. The rotor was cooled down to 25 K with helium gas in the center, and was spun with room temperature nitrogen gas on the side. The sample temperature was calibrated by measuring the spin-lattice relaxation time of ^{79}Br , as demonstrated by Thurber *et al.*^{5,6} Continuous-wave μw was irradiated from tuneable Virginia Diode Inc. source, with a frequency range of 193-201 GHz and μw irradiation power up to 350 mW, measured at right after AMC transmitter. The transmitted μw beam was guided through QO bridge, and finally reached to the corrugated wave-guide inside the 6.9 T wide bore magnet. The sample rotor (MAS-Stator) was located at the end of the wave-guide. The design of the probe was an adaptation from the design of Thurber *et al.*^{5,6} More detailed description can be found in a recent publication from Han group.⁷

T_{1e} Measurement

The T_{1e} relaxation time was measured for Trityl and TEMPO at DNP conditions using saturation recovery experiment. The pulse scheme is shown in Fig. S1(a). 100 ms, $P_{\mu w} = 120$ mW μw pulse was used to saturate the electron spins at the probe frequency, ν_{probe} . The EPR signal intensity was recorded at the same frequency using solid-echo detection, following a variable recovery delay, τ_D . T_{1e} was measured for three different radical mixtures, (a) TEMPO:Trityl = 1:1 ($C_{total} = 30$ mM, blue), (b) 2:1 ($C_{total} = 30$ mM, red). Two-component exponential fitting, using the equation, $I = I_0(1-A^*(\exp(-\tau_D/T_{1e-slow}))-B^*(\exp(-\tau_D/T_{1e-fast})))$, was used to extract the T_{1e} values recorded for ν_{probe} set to the center frequencies of the Trityl (Fig. S1 solid lines) and TEMPO (Fig. S1 dotted lines) radicals. We make

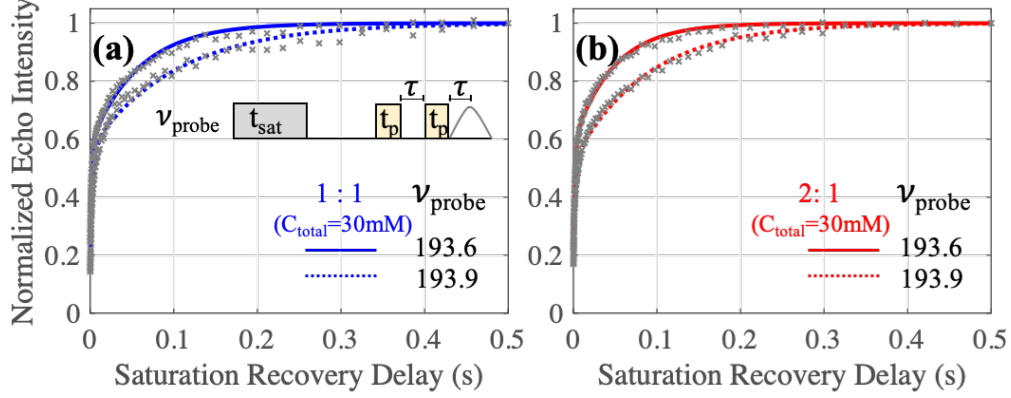


Figure S1: Saturation recovery T_{1e} measurement at 4 K for two different radical-mixtures: (a) TEMPO:Trityl = 1:1 ($C_{total} = 30$ mM, blue), (b) 2:1 ($C_{total} = 30$ mM, red). The grey crosses are normalized electron echo intensities as a function of τ_D , and the solid and dotted lines are the two-component fitting curve for ν_{probe} set at Trityl (193.6 GHz) and TEMPO (193.9 GHz) center frequencies, respectively.

two major observations: (i) with the same total spin concentration, T_{1e} measured at Trityl and TEMPO frequencies barely changed with the radical compositions; (ii) T_{1e} of Trityl was significantly shorter than that of TEMPO for both ratios. In the 1:1 ratio, the average T_{1e} values were 32.7 ± 3.6 ms and 54.8 ± 9.2 ms for Trityl and TEMPO, respectively. This is unexpected, and suggests that the benefit for DNP of mixing Trityl with TEMPO does not come from more facile saturability of the Trityl resonance under these condition. Fitted T_{1e} are recorded in Table S1, where T_{1e} are calculated as $(A * T_{1e-slow} + B * T_{1e-fast}) / (A + B)$.

Table S1: Simulated T_{1e}

TEMPO:Trityl (C_{total} mM)	ν_{probe} (GHz)	$T_{1e-slow}$ (ms)	A	$T_{1e-fast}$ (ms)	B	T_{1e} (ms)
1:1 (30)	193.6	58.0 ± 3.4	0.418 ± 0.01	1.4 ± 0.1	0.339 ± 0.01	32.7 ± 3.6
1:1 (30)	193.9	103.3 ± 8.8	0.432 ± 0.02	3.4 ± 0.4	0.407 ± 0.01	54.8 ± 9.2
2:1 (30)	193.6	48.0 ± 2.4	0.411 ± 0.01	1.8 ± 0.1	0.374 ± 0.01	26.0 ± 2.6
2:1 (30)	193.9	87.8 ± 5.3	0.476 ± 0.01	2.5 ± 0.3	0.345 ± 0.01	52.0 ± 5.6

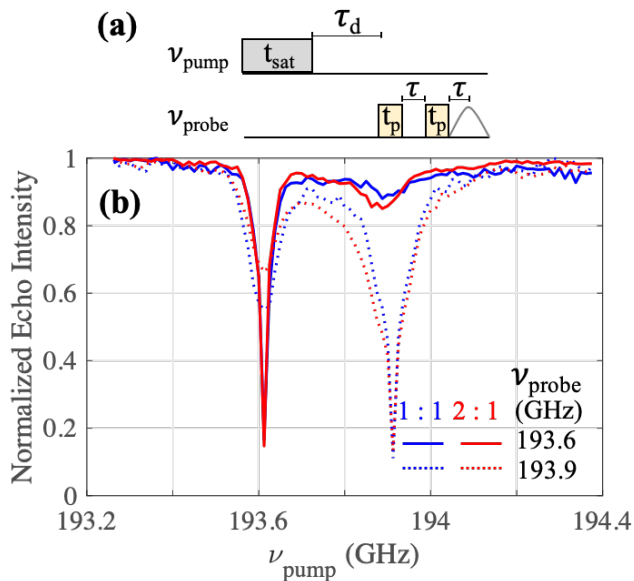


Figure S2: ELDOR experiments with a pulse scheme (a) were recorded at 4 K for mixed-radical systems (b) TEMPO:Trityl = 1:1 (blue) and 2:1 (red) with a total concentration of 30 mM. Solid and dotted lines correspond to $\nu_{\text{probe}} = 193.6$ and 193.9 GHz, respectively. The amplitude for the 100 ms ν_{pump} is 120 mW.

Pump-probe ELDOR experiment

ELDOR experiments delineate how e spin saturation at one frequency (ν_{pump}) is transferred to another frequency (ν_{probe}) across the EPR line. ELDOR profiles are shown in Fig. S2 for the 1:1 (blue) and 2:1 (red) ratios, where the solid and dotted lines correspond to $\nu_{\text{probe}} = 193.6$ and 193.9 GHz, respectively. The ELDOR spectra of the two mixtures at $\nu_{\text{probe}} = 193.6$ GHz display comparable eSD around the Trityl, indicating similar e spin dipolar coupling from clustering of Trityl in DNP-juice.⁸ When ν_{probe} is set to 193.9 GHz, the ELDOR profile of the 2:1 sample exhibits greater eSD around the TEMPO ν_{pump} frequency than in the 1:1 sample, indicating the eSD among TEMPO has increased. Meanwhile, for $\nu_{\text{probe}} = 193.9$ GHz, smaller eSD is observed in the 2:1 mixture when the ν_{pump} is set around the Trityl frequency, which can be explained by the relatively lower spin density of Trityl. Taken together, the ELDOR data analysis suggests that the benefit of the 2:1 mixture mainly comes from a higher number density of CE-fulfilling spins, as properties of spin dynamics and saturation appear rather comparable for the two ratios.

Numerical simulation

Easy Spin Simulation

The electron spectra of TEMPO and Trityl radicals, shown in Fig. 1 of the manuscript where simulated using Easyspin simulation package.⁹ The g and A tensors are mentioned in Table S2.

Table S2: g and A anisotropy

Radical	g_x	g_y	g_z	A_x MHz	A_y MHz	A_z MHz
TEMPO	2.009	2.006	2.0021	16	15	95
Trityl	2.0034	2.0031	2.0027	0	0	0

CE-DNP Simulation under MAS using Spin Evolution

The Cross-Effect DNP simulations of mixed radical system were performed using Spin-Evolution software package, under 10 kHz MAS, 100 K and 6.9 T conditions.¹⁰ The Spin-Evolution package allows DNP simulation for solid samples with powder averaging in Liouville space, and therefore can also incorporate relaxation into account. The simulations were performed for $e_1 - e_2 - {}^1\text{H}$ and $e_1 - e_2 - e_3 - {}^1\text{H}$ spin system, with e_1 representing a narrow-line Trityl radical, and e_2 and e_3 representing broad-line TEMPO radicals. The principal axis components of the g-tensors of the electron spins were taken the same as in Table S2. The g-tensor of e_2 and e_3 were related to e_1 by the Euler angles sets, (30,10,0) and (50,70,0), respectively. The relative e_1 - e_2 and e_1 - e_3 dipolar tensor orientation were given by the angles (20,60,30) and (50,90,60), respectively. The orientation of the dominant $e_1 - {}^1\text{H}$ hyperfine coupling was chosen to be (40,10,0). The relaxation rates, T_{1H} , T_{1e_1} , and $T_{1e_{2/3}}$, are set to 4 s, 4 ms, and 3 ms respectively, unless mentioned otherwise.

Mixed-radical DNP Frequency Profile

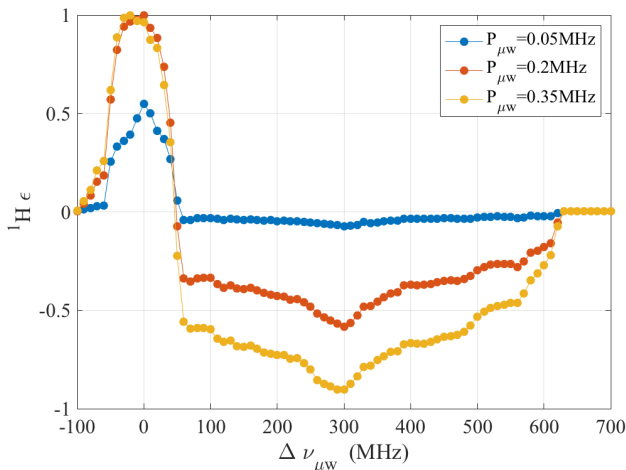


Figure S3: Numerically simulated, normalized ^1H DNP frequency profile using $e_1 - e_2 - ^1\text{H}$ spin system for three different μw power, 0.05 MHz, 0.2 MHz, and 0.35 MHz. The simulation was performed at 10 kHz spinning using T_{1e} of 3 ms and 1 ms for e_1 and e_2 , respectively.

The ^1H DNP enhancement, for $e_1 - e_2 - ^1\text{H}$ system, as a function of μw frequency offset with respect to the center of Trityl, is shown in Fig. S3 for three different μw powers. As evident from the figure, at low μw power, significant CE enhancement is obtained only at the Trityl resonance frequency. As the μw power increases, saturation of TEMPO can also lead to large enhancement.

DNP Enhancement Comparison for 1:1 and 2:1 Ratios.

The ^1H DNP enhancement, for $e_1 - e_2 - ^1\text{H}$ (TEMPO:Trityl = 1:1) system and $e_1 - e_2 - e_3 - ^1\text{H}$ (TEMPO:Trityl = 2:1) system at the optimum μw frequency condition, simulated at 10 kHz is shown in Fig. S4. As evident from the figure, $^1\text{H}\epsilon$ increased statistically for most orientations at the 2:1 ratio.

Nuclear spin depolarization under MAS

Thurber *et al.*¹¹ and Mentink-Vigier *et al.*^{12,13} have demonstrated the nuclear spin depolarization effect of the CE DNP mechanism under MAS in the absence of microwave irradiation.

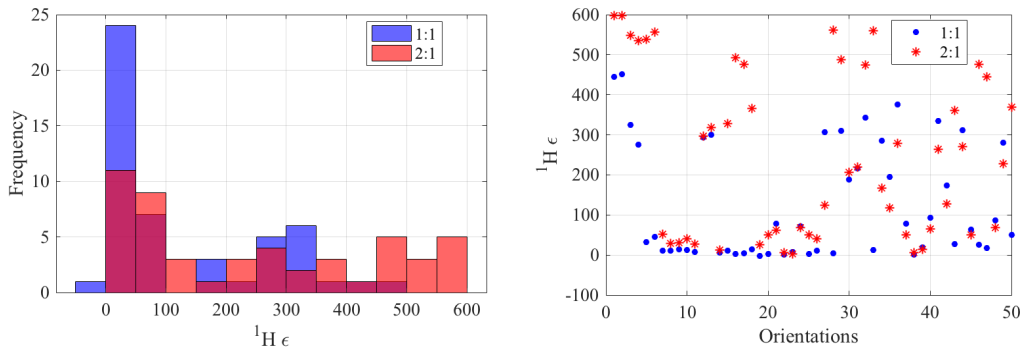


Figure S4: Numerically simulated ${}^1\text{H}\epsilon$ for $e_1 - e_2 - {}^1\text{H}$ (blue) and $e_1 - e_2 - e_3 - {}^1\text{H}$ (red) spin systems at 6.9 T, 10 kHz MAS and 0.2 MHz $P_{\mu\nu}$. $e_1 - e_2$, $e_1 - e_3$ and $e_1 - {}^1\text{H}$ dipolar couplings are fixed to 6 MHz, 6 MHz, and 2 MHz, respectively. (a) Histogram distribution of enhancement for 50 different molecular orientations in a powder. (b) ${}^1\text{H}$ DNP enhancement for the individual orientations.

Recently, Lund *et al.*⁷ experimentally illustrated the role of T_{1e} on nuclear depolarization by systematically changing the local and global electron spin concentration using mono-, bi- and tri-radicals. Putting together all these studies, we have learned that depolarization effects are primarily modulated with the electrons T_{1e} rates. However, it has also been demonstrated by Mentik-Vigier *et al.* that separation in the isotropic g of the two electrons can minimize the depolarization effect. Validating this argument, the mixed TEMPO-Trityl radical has also been shown to exhibit minimal ${}^1\text{H}$ depolarization¹³ in contrast to AMUPOL or other tethered bis- or tris-nitroxide radicals.^{7,12}

In the context of the study presented here, an intriguing question arises- Will the 2:1 (TEMPO:Trityl) type mixed radical PA have an increased depolarization effect as a result of TEMPO-TEMPO coupling? To address this question, we have performed simulations on a tethered 2:1 PA and monitored ${}^1\text{H}\epsilon_{depo} = {}^1\text{H}\text{-signal}_{Spin}/{}^1\text{H}\text{-signal}_{Static}$ at 10 kHz MAS as a function of TEMPO(e_2)-TEMPO(e_3) dipolar coupling (Fig.S5). In simulation, we have found that introducing $e_2 - e_3$ coupling increases depolarization since the $e_2 - e_3$ CE mechanism becomes operational. However, the increase is only up to $\sim 12\%$ for an intermediate $e_2 - e_3$ dipolar coupling. Weaker or stronger $e_2 - e_3$ couplings will attenuate depolarization effect as discussed earlier in the literature by Lund *et al.*⁷ We want to assert that the exact value

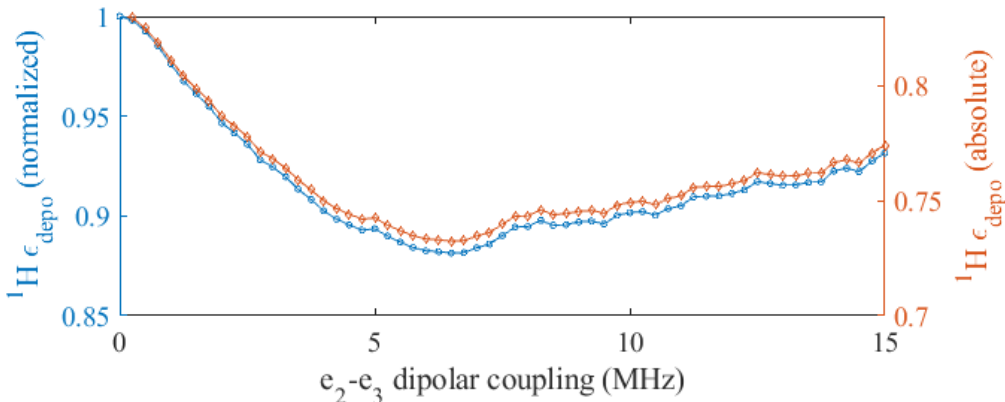


Figure S5: Numerically simulated ${}^1\text{H}\epsilon_{\text{depo}}$ as a function of $e_2 - e_3$ dipolar coupling for $e_1 - e_2 - e_3 - {}^1\text{H}$ spin systems at 6.9 T and 10 kHz MAS. $e_1 - e_2$ and $e_1 - e_3$ dipolar couplings are fixed to 15 MHz. $e_1 - \text{H}$ and $e_3 - \text{H}$ dipolar couplings are set to 2 MHz. T_{1e} was set to 1 ms for all the electron spins. The left y-axis shows ${}^1\text{H}\epsilon_{\text{depo}}$ normalized with respect to zero $e_2 - e_3$ coupling. Right y-axis shows absolute depolarization value.

of depolarization for tethered spin system is not easy to predict or determine as there are cornucopia of parameters (T_{1e} , g-tensor and relative orientations, $e-e$ couplings) governing the extent of depolarization. Overall, we also think that the added benefit of TEMPO-TEMPO CE enhancement (μw -on condition) will curb any of its depolarization effect.

References

- (1) Siaw, T. A.; Leavesley, A.; Lund, A.; Kaminker, I.; Han, S. *J. Magn. Reson.* **2016**, *264*, 131–153.
- (2) Kaminker, I.; Barnes, R.; Han, S. *J. Magn. Reson.* **2017**, *279*, 81–90.
- (3) Leavesley, A.; Kaminker, I.; Han, S. *eMagRes* **2018**, 133–154.
- (4) Equbal, A.; Li, Y.; Leavesley, A.; Huang, S.; Rajca, S.; Rajca, A.; Han, S. *J. Phys. Chem. Lett.* **2018**, *9*, 2175–2180.
- (5) Thurber, K. R.; Potapov, A.; Yau, W.-M.; Tycko, R. *J. Magn. Reson.* **2013**, *226*, 100–106.

- (6) Thurber, K.; Tycko, R. *J. Magn. Reson.* **2016**, *264*, 99–106.
- (7) Lund, A.; Equbal, A.; Han, S. *Phys. Chem. Chem. Phys.* **2018**, *20*, 23976–23987.
- (8) Weber, E. M.; Sicoli, G.; Vezin, H.; Frébourg, G.; Abergel, D.; Bodenhausen, G.; Kurzbach, D. *Angew. Chem., Int. Ed.* **2018**, *57*, 5171–5175.
- (9) Stoll, S.; Schweiger, A. *J. Magn. Reson.* **2006**, *178*, 42–55.
- (10) Veshtort, M.; Griffin, R. G. *J. Magn. Reson.* **2006**, *178*, 248–282.
- (11) Thurber, K. R.; Tycko, R. *J. Chem. Phys.* **2014**, *140*, 184201–184211.
- (12) Mentink-Vigier, F.; Paul, S.; Lee, D.; Feintuch, A.; Hediger, S.; Vega, S.; De Paëpe, G. *Phys. Chem. Chem. Phys.* **2015**, *17*, 21824–21836.
- (13) Mentink-Vigier, F.; Mathies, G.; Liu, Y.; Barra, A.-L.; Caporini, M. A.; Lee, D.; Hediger, S.; Griffin, R. G.; De Paëpe, G. *Chem. Sci.* **2017**, *8*, 8150–8163.